ACS APPLIED ENERGY MATERIALS

www.acsaem.org Article

Dopant-Free Mexylaminotriazine Molecular Glass Hole Transport Layer for Perovskite Solar Cells

LiangLe Wang, Md. Shahiduzzaman,* E. Y. Muslih, Masahiro Nakano, Makoto Karakawa, Koji Tomita, Olivier Lebel, Jean Michel Nunzi,* and Tetsuya Taima*

Cite This: *ACS Appl. Energy Mater.* 2021, 4, 12232−12242 Read Online

ACCESS | Metrics & More | Article Recommendations | Supporting Information

ABSTRACT: The development of dopant-free organic hole transport materials (HTMs) is critical to the commercialization of perovskite solar cells (PSCs). Indeed, dopants are the key determinants for reducing photovoltaic stability. Here, we designed and synthesized three mexylaminotriazine molecular glass derivatives containing triphenylamino moieties with an easy and low-cost process. All three compounds show good solubility and film-forming ability, and they show promising results as HTMs in PSCs. The PSCs fabricated with these mexyaminotriazine-substituted HTMs reach efficiencies up to [power conversion efficiency (PCE)] 12.50% (12.40% stabilized). Furthermore, we also measured the long-term stability of PSCs using these HTMs, and the devices showed no significant decrease of their initial PCE after storage in the dark under an atmospheric environment with a relative humidity range of 40 to 50% for over 1000 h. This work indicates that methylaminotriazine derivatives are potential hole transport layer candidates for PSCs and provides strategic guidance for the further design of dopant-free HTMs.

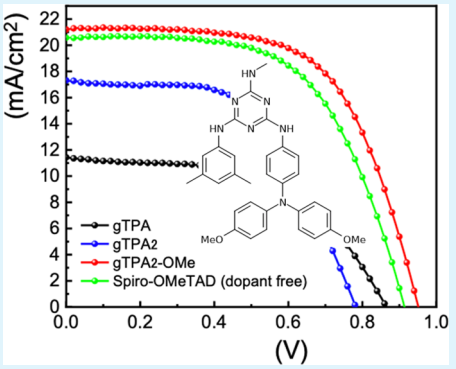

KEYWORDS: *perovskite solar cell, methylaminotriazine derivative, molecular glass, dopant-free, hole transport material*

INTRODUCTION

Organic−inorganic halide hybrid perovskite solar cells (PSCs) are the utmost encouraging photovoltaic technologies for future commercialization owing to their simplicity, low fabrication cost, and flexibility. They are also considered as leaders of the third-generation photovoltaic cells after crystalline silicon and thin-film solar cells. Hybrid organic−inorganic PSCs have unique photovoltaic characteristics, including adjustable band gap, strong and wide light absorption, excellent electron mobility, and long carrier diffusion length and lifetime.[1−7] In 2009, Japanese scientists Miyasaka et al. took the lead in using perovskite materials for dye-sensitized solar cells as light-absorbing materials, with methylammonium lead iodide ($CH_3NH_3PbI_3$, $MAPbI_3$)-sensitized TiO_2 as the anode, to obtain a power conversion efficiency (PCE) of 3.8%.[8] In 2011, Park and his group increased the conversion efficiency to 6.5% through technical improvements.[9] However, all the devices reported at that stage showed extremely poor stability. In 2012, Lee and Snaith introduced the hole transport material (HTM) 2,2′,7,7′-tetrakis-(*N*,*N*-di-*p*-methoxy-phenylamine)-9,9′-spirobifluorene (spiro-OMeTAD), which improved the efficiency of the solid-state PSCs up to 10%.[10] More importantly, the unencapsulated device showed excellent stability: the photovoltaic performance was not significantly degraded after 500 h. Since then, PSCs have received a great deal of attention, and according to recent reports, PSCs have reached a record efficiency of 25.5%.[11]

The hole transport layer (HTL) has a great significance as an important part of the PSC and is involved in the efficient extraction of photogenerated holes, inhibiting the direct contact between the perovskite and metal electrode (e.g. Ag, Au, and Al) and suppressing the charge recombination losses.[12,13] At present, according to their material properties, the HTMs can be roughly divided into organic polymers [e.g. poly(4-butyltriphenylamine), commonly known as poly(TPD), and poly(3-hexylthiophene-2,5-diyl), commonly known as P3HT],[11,14−17] small organic molecules (e.g. tetra{4-[*N*,*N*-(4,4′-dimethoxydiphenylamino)]phenyl}ethene and 3,4-ethylenedioxythiophene),[18,19] and inorganic materials (e.g. CuI, CuO_x, NiO, V_2O_5, and CuSCN).[20−28] The most commonly used one is organic small-molecule materials because of the processing conditions, which are highly compatible with the perovskites.[29] Spiro-OMeTAD and polytriarylamine (PTAA) are the most commonly used HTMs for PSCs, which can usually provide an efficiency higher than 22%. However, the production conditions of spiro-OMeTAD are complicated, requiring five synthesis steps and an ultra-low temperature

Received: July 9, 2021
Accepted: October 11, 2021
Published: October 20, 2021

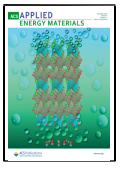

https://doi.org/10.1021/acsaem.1c02013
ACS Appl. Energy Mater. 2021, 4, 12232−12242

(−78 °C),[30] which make spiro-OMeTAD expensive ($300 USD/g), and the cost of PTAA is twice that of spiro-OMeTAD. In addition to that, the use of spiro-OMeTAD materials generally requires doping with lithium bis-(trifluoromethylsulfonyl)imide (Li-TFSI) and 4-*tert*-butylpyridine (4-*t*BP). It was also reported that dopants will affect the stability of the devices.[31] Therefore, the development of low-cost dopant-free HTL materials is extremely important for the developing PSC industry.

Organic small-molecule materials are regarded as the most suitable materials to replace spiro-OMeTAD due to their advantages, including well-defined molecular weight, the ability to passivate the defects of the perovskite surface, and high repeatability, which have been widely studied. Triarylamines (such as triphenylamine, and TPA), as groups with good stability and solubility, are often used as building blocks for small organic molecule HTMs. As early as 2014, Ko fabricated new types of HTMs named tris{*N*,*N*-bis((4-methoxyphenyl)-amino)biphenyl}-amine (OMeTPA-TPA) and tris{*N*,*N*-bis-((4′-methoxyphenyl)amino)phenyl}-fused amine (OMeTPA-FA) with the planar TPA as the side or core unit. They applied it to PSCs, and the PSCs with OMeTPA-FA achieved the best PCE of 13.63%, which is comparable to devices with spiro-OMeTAD (14.68%).[32] There have been many reports of small molecules based on 9,9′-spirobifluorene, thiophene, triazatruxene, and carbazole as HTMs for PSCs.[33−36] In all these cases, the role of the core is to prevent the crystallization of the TPA moieties. However, to the best of investigators' knowledge, the study on mexylaminotriazine as the core of the HTM is very scarce. Mexylaminotriazine derivatives are able to form very stable glasses and are easily functionalizable. Therefore, the methylaminotriazine group became an attractive building block to easily design and synthesize HTMs that form amorphous thin films without crystallization.[37]

In 2017, Nunzi and Lebel et al. used the 3,4,9,10-perylenetetracarboxylicdiimide-functionalized mexylaminotriazine derivative (PDI-glass) as a thin-film layer to modify the interface of the electron transport layer TiO_x for the first time, for which the PCE increased by 39%.[38] Then, they added PDI-glass and diketopyrrolopyrrole (DPP-glass) as guest acceptors into poly(3-hexythiophene) (P3HT) and [6,6]-phenyl-C_{61}-butyric acid methyl ester ($PC_{61}BM$) to obtain ternary blend organic solar cells with device performance improvements of 38 and 36%, respectively.[39]

Recently, our team synthesized a new type of methylaminotriazine derivative (herein named gTPA) by a simple condensation of 2-mexylamino-4-methylamino-6-(4-aminophenylamino)-1,3,5-triazine and *N*-(4-formylphenyl)-diphenylamine. In order to study the photoelectric properties of the material, we conducted a systematic study on the film thickness of gTPA and achieved a PCE of 2.92% on the traditional $MAPbI_3$-based PSCs.[40] To conduct a more in-depth study of this very promising structure (methylaminotriazine) as a HTM for PSCs, we synthesized two novel TPA-containing mexylaminotriazine derivatives (named gTPA2 and gTPA2-OMe, Scheme 1) and systematically compared the effect of these three materials on the performance of PSCs. The resulting materials exhibit excellent solubility and film-forming ability in common solvents. We conducted a systematic study of the thermal, optical, and optoelectronic properties of these materials and successfully applied these materials as HTLs for PSCs. Among them, gTPA2-OMe yielded the best-performing PSCs, showing a PCE as high as 12.50% (12.40% stabilized

Scheme 1. Molecular Structures of gTPA, gTPA2, and gTPA2-OMe

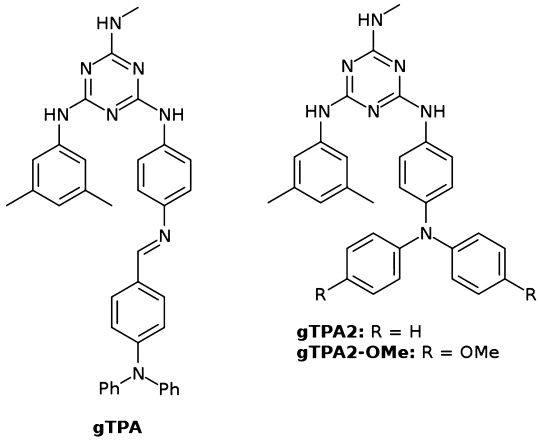

efficiency), which is a little higher than that of dopant-free spiro-OMeTAD devices. The projected synthetic cost of these materials is in the 10$/g range, which is much lower than spiro-OMeTAD. In addition, they also show outstanding stability. After nearly 1000 min of continuous light soaking (AM 1.5 G illumination), gTPA2-OMe-based PSCs maintain nearly 90% of their initial efficiency. They also exhibit better long-term stability (no significant decrease in their initial PCE after being stored in a dark ambient atmosphere with a humidity range of 40−50% for over 1000 h). These molecular glasses reveal a very promising potential for commercial applications of PSCs.

EXPERIMENTAL SECTION

Synthesis. *General.* 2-Mexylamino-4-methylamino-6-(4-aminophenylamino)-1,3,5-triazine,[37] 2-chloro-4-methylamino-6-mexylamino-1,3,5-triazine, *N*-(4-aminophenyl)diphenylamine,[41] *N*-(4-aminophenyl)-*N*,*N*-bis(4-methoxyphenyl)amine,[42] and gTPA[40] were synthesized as described in the literature. All the commercially available reagents and solvents were purchased and used without further purification. Fourier transform infrared (FTIR) spectroscopy spectra were obtained with thin films cast from CH_2Cl_2 on KBr windows using a PerkinElmer Spectrum 65 spectrometer. ^1H and ^{13}C NMR spectra were obtained using a 300 MHz Varian Oxford or a 400 MHz Bruker AV400 spectrometer at 298 K unless noted otherwise. A TGA 2950 thermogravimetric analyzer (TA Instruments) at a heating rate of 50 °C/min under a nitrogen atmosphere was used to analyze decomposition of molecular glasses. T_g, T_c, and T_m were measured by differential scanning calorimetry (DSC) with a TA Instruments 2010 or a TA Instruments Q20 calorimeter calibrated with indium at a heating rate of 5 °C/min. Transition temperatures were described after an opening cycle of heating and cooling.

Synthesis of gTPA2. 2-Chloro-4-methylamino-6-mexylamino-1,3,5-triazine (0.625 g, 2.37 mmol) and *N*-(4-aminophenyl)-diphenylamine (0.649 g, 2.49 mmol) were dissolved in tetrahydrofuran (THF, 10 mL) in a round-bottomed flask equipped with a magnetic stirrer and a water-jacketed condenser. The mixture was then refluxed for 12 h, at the end of which the volatiles were removed under vacuum, and CH_2Cl_2 and 1 M aqueous HCl were added. Both layers were detached; the aqueous layer was extracted once more with CH_2Cl_2, and then, the organic extracts were washed with aqueous $NaHCO_3$, dried over Na_2SO_4, filtered, and dried under vacuum. The residue was purified on a short silica pad using AcOEt/hexanes (2:8 to remove the starting materials and then 7:3 to recover the product). 0.754 g of compound gTPA was thus obtained (1.55 mmol, 65%). T_g 91 °C; FTIR (CH_2Cl_2/KBr): 3410, 3275, 3179, 3058, 3032, 2946, 2915, 1586, 1504, 1421, 1361, 1313, 1269, 1232, 1181, 835, 808, 750,

https://doi.org/10.1021/acsaem.1c02013
ACS Appl. Energy Mater. 2021, 4, 12232−12242

Scheme 2. Synthesis of gTPA2 and gTPA2-OMe

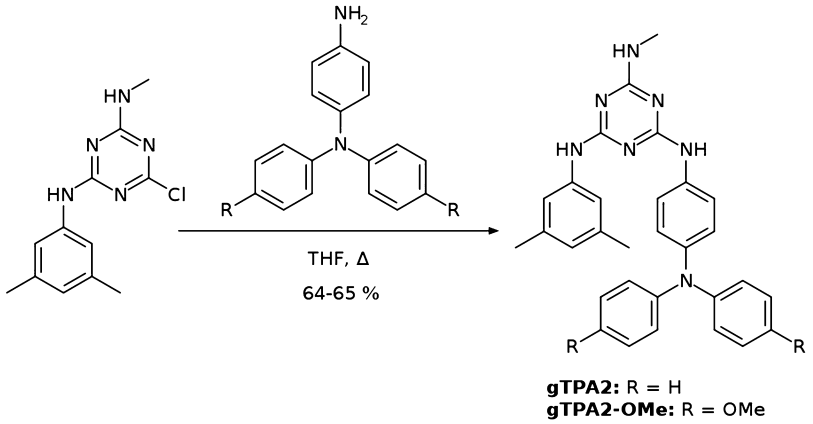

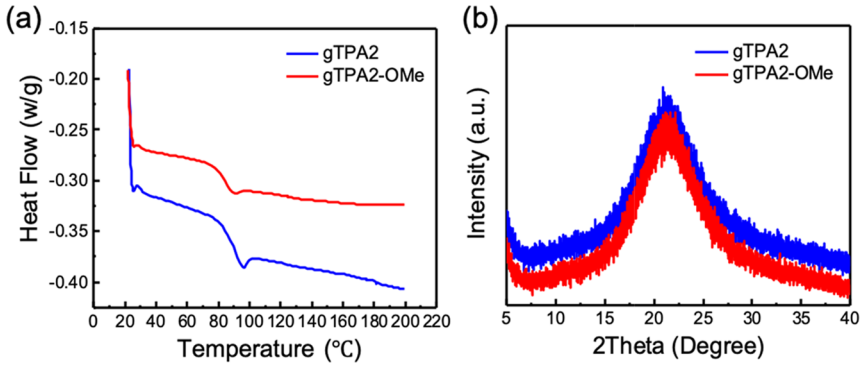

Figure 1. (a) DSC scans of gTPA2 and gTPA2-OMe measured at a heating rate of 5 °C/min after an opening heating−cooling cycle. The exotherm is directed uphill. (b) XRD spectra of the gTPA2 and gTPA2-OMe deposited as thin films on a glass substrate.

694 cm^{-1}; ^1H NMR (300 MHz, DMSO-d_6, 363 K): δ 8.73 (s, 1H), 8.51 (s, 1H), 7.77 (d, J = 8.8 Hz, 2H), 7.41 (s, 2H), 7.26 (t, J = 7.6 Hz, 4H), 7.01 (t, J = 7.8 Hz, 8H), 6.60 (s, 1H), 6.56 (d, J = 4.5 Hz, 1H), 2.91 (d, J = 4.5 Hz, 3H), 2.23 (s, 6H) ppm; ^{13}C NMR (75 MHz, C_6D_6): δ 166.0, 164.1, 163.8, 147.4, 140.7, 140.0, 137.0, 136.3, 129.1, 125.2, 123.0, 122.6, 121.9, 121.1, 117.6, 27.2, 21.1 ppm; HRMS (ESI, MH^+): calcd for $C_{30}H_{30}N_7$ (m/z), 488.2557; found, 488.2576.

Synthesis of gTPA2-OMe. Compound gTPA2-OMe was synthesized from 2-chloro-4-methylamino-6-mexylamino-1,3,5-triazine (4.68 g, 17.6 mmol) and *N*-(4-aminophenyl)-*N*,*N*-bis(4-methoxyphenyl)amine (5.65 g, 17.6 mmol) following the same procedure as for compound gTPA, thereby yielding 6.19 g of the title compound (11.3 mmol, 64%). T_g 85 °C; FTIR (CH_2Cl_2/KBr): 3405, 3278, 3178, 3036, 2996, 2951, 2833, 1604, 1575, 1503, 1424, 1360, 1316, 1266, 1238, 1179, 826, 808, 734, 576 cm^{-1}; ^1H NMR (300 MHz, DMSO-d_6, 363 K): δ 8.58 (s, 1H), 8.45 (s, 1H), 7.62 (d, J = 8.9 Hz, 2H), 7.37 (s, 2H), 6.95 (d, J = 9.0 Hz, 4H), 6.87 (d, J = 9.0 Hz, 4H), 6.82 (d, J = 8.9 Hz, 2H), 6.58 (s, 1H), 6.49 (d, J = 4.8 Hz, 1H), 3.75 (s, 6H), 2.87 (d, J = 4.8 Hz, 3H), 2.21 (s, 6H) ppm; ^{13}C NMR (75 MHz, C_6D_6): δ 166.0, 164.0, 163.8, 154.8, 142.4, 141.0, 140.0, 137.0, 134.3, 125.0, 123.0, 121.9, 121.2, 117.5, 114.7, 55.1, 27.2, 21.1 ppm; HRMS (ESI, MNa^+): calcd for $C_{32}H_{33}NaN_7O_2$ (m/z), 570.2588.2557; found, 570.2570.

Device Fabrication. A patterned fluorine-doped tin oxide (FTO)-glass substrate was sequentially cleaned by sonication with a commercial detergent in water, deionized water, and KOH solution for 15 min. The cleaned FTO-glass substrate was treated with oxygen plasma for 20 min prior to use. A 40 nm TiO_2 compact layer (CL) was deposited on the FTO-glass substrate.[43] Brookite TiO_2 nanoparticle (NP) colloidal suspension was spun-cast on the TiO_2 CL by spin-coating at 2000 rpm for 30 s and then thermal-treating at 105 °C for 5 min on a hot plate, followed by annealing at 180 °C for 60 min in a muffle furnace.[44,45] The detailed procedure for perovskite precursor solution making and spin-coating is reported elsewhere.[46]

All the HTM precursor solutions were spin-coated on the $MAPbI_3$ perovskite film at 4000 rpm for 30 s. Solutions of gTPA, gTPA2, gTPA2-OMe, and spiro-OMeTAD in chlorobenzene solution (CB) were prepared by dissolving 10 mg of gTPA, gTPA2, or gTPA2-OMe or 72.3 mg of spiro-OMeTAD in 1 mL of CB by stirring at room temperature for 6 h (Figure S1), respectively. The effect of different molecular glass film thicknesses on the performance of the device has been discussed in the previous work.[40] 100 nm Au was deposited on the HTL for completing the design of the device. The active area of the PSC was 9 mm^2. The optimized thicknesses of TiO_2 CL, BK TiO_2 NP layer (three cycle-coating was optimum), perovskite layer, TPA glass layer, and Au layer were measured to be ∼40, ∼120, ∼450, ∼80, and ∼100 nm thick Au electrode layer.

Characterization. The morphological and structural analyses were carried out using field emission scanning electron microscopy (FE-SEM; S-4800, Hitachi High-Tech, Tokyo, Japan) and an X-ray diffractometer (D8 Discover, Bruker AXS GmbH, Karlsruhe, Germany) with an X-ray tube (Cu Kα radiation, λ = 1.5406 Å). Light absorption in the three compounds (gTPA, gTPA2, and gTPA2-OMe) was characterized by ultraviolet−visible (UV−vis) and near infrared absorption spectroscopy (V-670, Jasco Corporation, Tokyo, Japan). The charge transport properties of perovskite and perovskite/HTL films were studied by photoluminescence (PL) (FP-8600, Jasco Corporation, Tokyo, Japan). The current density versus voltage (J−V) characteristics of the devices was studied in forward-bias (−0.2 to 1.2 V) and reverse-bias (1.2 to −0.2 V) modes at a scan speed of 0.05 V/s under simulated air mass (AM) 1.5 G illumination using a solar simulator at 100 mW/cm^2 and a Keithley 2401 digital source meter. The incident photon-to-electron conversion efficiencies (IPCEs) of the devices were recorded using a monochromatic xenon arc light system (Bunkoukeiki, SMI-250JA). The geometry of

https://doi.org/10.1021/acsaem.1c02013
ACS Appl. Energy Mater. 2021, 4, 12232−12242

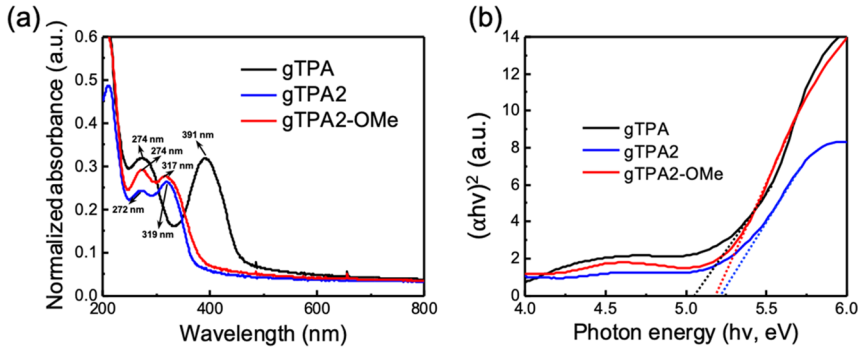

Figure 2. (a) UV−vis patterns of the different HTMs as thin films. (b) Tauc plot to estimate the band gap of the different HTMs.

Table 1. Photophysical, Thermal, and Semiconducting Characteristics of gTPA, gTPA2, and gTPA2-OMe

HTM	E_g (eV)	E_{HOMO} (eV)	E_{LUMO} (eV)	T_g (°C)	conductivity (S/cm)	mobility (cm^2/V·s)
gTPA	3.52[a]/5.08[b]	−4.89	1.37	93	3.3×10^{-4}	2.43×10^{-4}
gTPA2	4.23[a]/5.45[b]	−4.72	−0.49	91	3.9×10^{-4}	2.66×10^{-4}
gTPA2-OMe	4.01[a]/5.38[b]	−4.40	−0.39	85	5.1×10^{-4}	2.82×10^{-4}

[a]DFT calculation: $E_{LUMO} = E_{HOMO} + E_g$. [b]Band gap ($E_g$) estimated from Tauc plots of the UV−vis absorption coefficient.

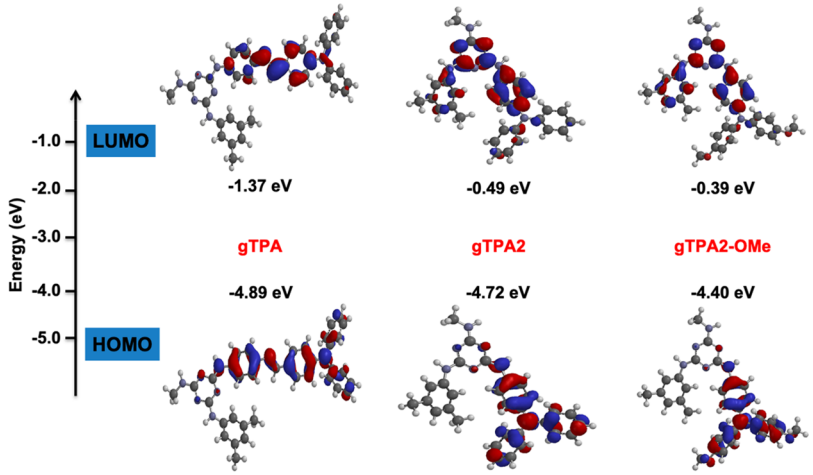

Figure 3. Energy level diagram of the HOMO and LUMO levels of gTPA, gTPA2, and gTPA2-OMe as simulated at the B3LYP/6-31G(d,p) level.

compounds gTPA, gTPA2, and gTPA2-OMe was optimized via density functional theory (DFT) calculations [B3LYP/6-31G(d,p)] with wave function Spartan '06 software to assess the energy levels of the highest occupied molecular orbital (HOMO) and lowest unoccupied molecular orbital (LUMO).

RESULTS AND DISCUSSION

Synthesis. gTPA was synthesized according to our previous work.[40] gTPA2 and gTPA2-OMe were synthesized by introducing the *N*-(4-aminophenyl)diphenylamine groups directly onto the triazine core by reacting the corresponding *N*-(4-aminophenyl)diphenylamines with 2-chloro-4-methylamino-6-mexylaminotriazine in refluxing THF, in 64−65% yields (Scheme 2). In both cases, the desired products could be purified on a short silica pad using AcOEt/hexane mixtures at varying ratios. Compound gTPA2-OMe contains additional electron-donating methoxy groups in the 4-position of the two other phenyl groups of the triarylamine group, similar to the benchmark HTL material spiro-MeOTAD.

Thermal, Optoelectrical, and Semiconducting Properties. As shown in Figure 1a, mexylaminotriazine derivatives gTPA2 and gTPA2-OMe are all capable of forming stable glasses at glass transition temperatures (T_g) of 91 and 85 °C, with no crystallization observed either by heating or prolonged standing at ambient temperatures. Compound gTPA2-OMe has a slightly lower T_g (85 °C) than its analogue gTPA2 because of the presence of flexible methoxy groups. No melting transitions were observed for any of the two gTPA2 analogues, as melting is associated with the presence of crystals, thereby revealing the lack of crystalline domains. To further demonstrate that these organic molecules are amorphous, we prepared solutions of the compounds and spin-coated the films on glass substrates. As shown in Figure 1b, all materials only display a large bulge at about $2\theta = 22°$, thereby confirming that the materials are completely amorphous. The wide-ranging X-ray diffraction (XRD) spectra at 22° are attributed to the p-stacking of the conjugated fragments that trouble charge transport.[47]

The normalized UV−vis absorption spectra of thin films of these three molecular glasses are shown in Figure 2a. Each of the three compounds (gTPA, gTPA2, and gTPA2-OMe) shows two absorption peaks at 274/391, 272/319, and 274/317 nm, respectively. Compared with gTPA2 and gTPA2-OMe, gTPA is significantly red-shifted. This is because gTPA

https://doi.org/10.1021/acsaem.1c02013
ACS Appl. Energy Mater. 2021, 4, 12232−12242

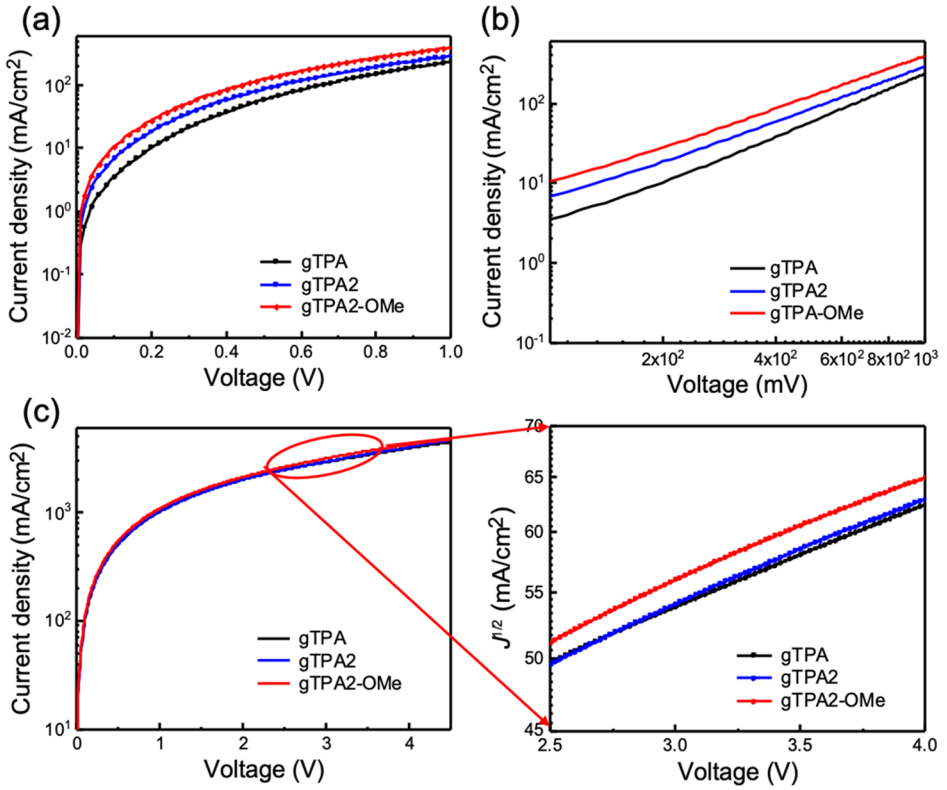

Figure 4. (a) $J-V$ curve of TPA glasses showing (a) conductivity and (c) hole mobility. (b) Dark $J-V$ curves received from hole-only devices with different HTMs. The hole-only devices prepared have the structure (FTO/HTM/Au). The inset shows the $J^{0.5}-V$ curve recorded from the SCLC region.

contains a more strongly conjugated system with imine and an additional phenyl ring. In contrast, gTPA2-OMe is significantly blue-shifted, indicative of a wider optical band gap, which is mainly related to the methoxy group on the side of gTPA2-OMe and provides higher tunability of its HOMO energy level.[29] According to the absorption coefficient, a Tauc plot of $(\alpha h\nu)^2$ versus $h\nu$ is used to determine the optical band gap,[48,49] as shown in Figure 2b. The optical band gaps of these three molecular glass materials were estimated from the Tauc relation, as shown in Table 1. gTPA2 and gTPA2-OMe both have a wide optical band gap (approximately 5.4 eV).

Aminotriazines are known to adopt several different conformations of similar energy, which interconvert slowly. In the present case, conformational equilibria are not expected to impact orbital energy levels as they involve remote groups. Therefore, DFT calculations were performed on a single conformation with both aryl groups pointing in the same direction. The HOMO and LUMO energy levels are listed in Table 1, and the frontier orbitals are displayed in Figure 3. Figure S2 shows an energy level diagram of novel HTMs with perovskite. We find that all three novel mexylaminotriazine HTMs match well with the energy levels of perovskite. Interestingly, the large energy barrier between the conduction band of the perovskite and the E_{LUMO} of the HTM can effectively prevent undesired photogenerated electron transfer, especially reducing the charge recombination rate at the perovskite/HTM interface.[50] From the calculations, the HOMO and LUMO energy levels increase from compound gTPA, which contains an electron-withdrawing imine group, to compound gTPA2-OMe, which is substituted with two electron-donating methoxy groups. Upon seeing the HOMO−LUMO gaps, compound gTPA2 shows the highest gap with 4.23 eV, followed by compounds gTPA2-OMe (4.01 eV) and compound gTPA (3.52 eV). The fact that compound gTPA shows the smallest calculated HOMO−LUMO gap can be rationalized by the fact that its chromophore contains an additional phenyl group. This is especially apparent in view of the HOMO orbital of compound gTPA, showing an extended HOMO orbital. Additionally, the LUMO orbital of compound gTPA is completely located on the chromophore itself, unlike compounds gTPA2 and gTPA2-OMe, in which the LUMO orbital is partially delocalized on the triazine ring.

We measured the conductivity (σ_0) and hole mobility (μ) of these three novel HTL molecular glasses. It should be noted that all materials are dopant free. The conductivity is obtained from the linear current density−voltage ($J-V$) curve in a hole-only device with the structure FTO/molecular-glass (optimized 80 nm thickness)/Au under dark and ambient conditions. The equation $\sigma_0 = JdV^{-1}$ is used to calculate σ_0 (Figure 4a). We also plotted in Figure 4b the $J-V$ curves on a log scale to reveal the hole-only device trap density. The calculation method for the defect density (N_t) is mentioned in our previous research.[46] It is difficult (Figure 4b) to obtain the trap-filled limit (TFL) voltage V_{TFL}, and the entire scanning voltage range (0−1 V) can almost be regarded as "trap-free" charge transport. The hole mobility of the three HTMs is obtained from the space-charge limited current method (Figure 4c), using the Mott−Gurney law ($J = 9\varepsilon\varepsilon_0\mu V^2/8d^3$). The fitted slope $J^{1/2}-V$ is shown in the zoomed portion of Figure 4c. The conductivity and hole mobility are calculated and listed in Table 1. gTPA2-OMe exhibits the highest conductivity and hole mobility, meaning that it carries the best potential as a hole-transfer material. In addition, the hole

https://doi.org/10.1021/acsaem.1c02013
ACS Appl. Energy Mater. 2021, 4, 12232−12242

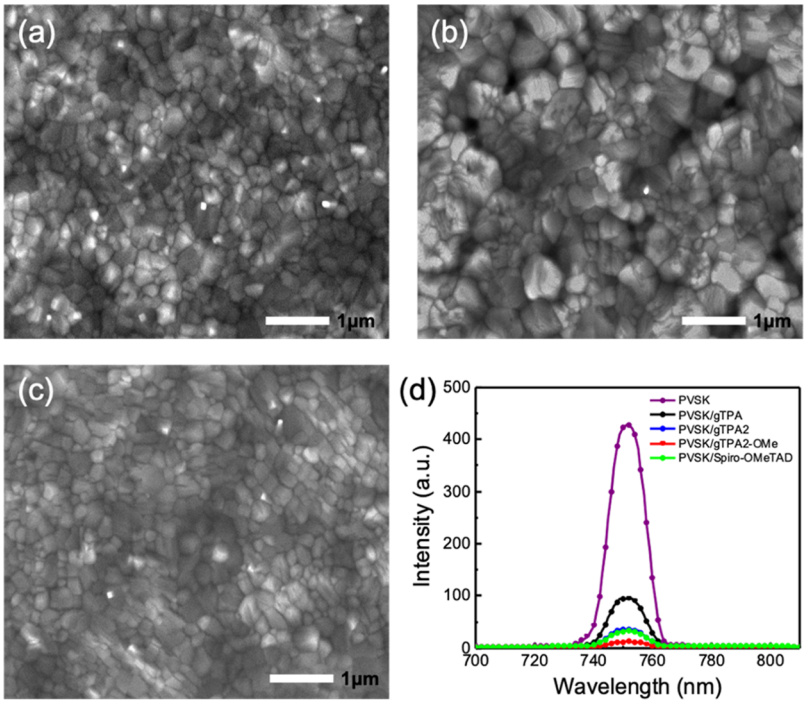

Figure 5. Top-view SEM images of perovskite with (a) gTPA, (b) gTPA2, and (c) gTPA2-OMe. (d) PL spectra of FTO/perovskite and FTO/perovskite with different TPA molecular glasses, with excitation at 500 nm.

mobilities of all three TPA glasses are mostly in similar ranges as the ones measured elsewhere for spiro-OMeTAD.[51]

The three molecular glasses were spin-coated on top of the perovskite to investigate their film-forming ability (Figure S3). All these three materials form smooth films on the perovskite, meaning that they all have good solubilities and form amorphous thin films. This is further verified by SEM (Figure 5). The perovskites coated with gTPA and gTPA2 are rougher than the one coated with gTPA2-OMe. Arguably, the smooth nature of the gTPA2-OMe film will improve the contact between the perovskite and HTM layer, thereby improving hole extraction. Additionally, avoiding direct contact between the perovskite layer and the electrode improves the performance of the devices.

Figure 5d exhibits the PL spectra of the perovskite film, both uncoated and coated with each of the TPA glasses. The pristine perovskite film shows a high-intensity peak (purple line). Upon coating the perovskite film with different HTMs, the PL intensity decreases. It was reported that such a quenching effect happens for steady-state PL.[52] Compared with the pristine perovskite film, the PL intensity drops around 22, 8, and 3%, respectively, after coating with gTPA, gTPA2, and gTPA2-OMe. We characterized the PL spectrum of FTO/perovskite/spiro-OMeTAD, as shown in Figure 5d (green-line). We see that the degree of PL quenched by undoped spiro-OMeTAD is equivalent to that of gTPA2 and both are lower that of gTPA2-OMe. Strong PL reduction signifies that the perovskite film coated by the HTM undergoes charge transfer at the interface between both layers; in addition, gTPA2-OMe appears to be more efficient in extracting holes from the perovskite and effective in impeding charge-carrier recombination. Quenching the PL intensity demonstrates that the novel molecular-glasses promote efficient charge collection like spiro-OMeTAD.

We fabricated n−i−p type devices with a structure of FTO/TiO_2 CL/BK TiO_2 NP/perovskite/molecular-glass/Au, by introducing gTPA, gTPA2, and gTPA2-OMe as well as spiro-OMeTAD as HTMs. The schematic diagram of the device is shown in Figure S4a. Figure S4b−d shows the cross-sectional SEM images of the optimized devices, in which we clearly distinguish the film thickness of each individual layer.

The $J-V$ curves with the varying configuration of TPA devices and IPCE spectra are shown in Figure 6a,b. The device parameters are summarized in Table 2. The device with gTPA2-OMe as a HTM under reverse bias shows a high PCE of 12.50%, with a short-circuit current density (J_{sc}) of 21.21 mA/cm^2, an open-circuit voltage (V_{oc}) of 0.95 V, and a fill factor (FF) of 0.62, which is comparable to the efficiency of devices using dopant-free spiro-OMeTAD (11.25%). We studied the hysteresis index (HI) of each device by measuring $J-V$ in both forward (FS) and reverse scan (RS) directions (Figure S5). The HI is usually calculated using the formula: $\mathrm{HI} = \frac{\mathrm{PCE}_{(\mathrm{reverse})} - \mathrm{PCE}_{(\mathrm{forward})}}{\mathrm{PCE}_{(\mathrm{reverse})}}$;[53] the HIs of both gTPA2-OMe and spiro-OMeTAD (dopant free) devices are 0.27 and 0.31. Both types of devices clearly show significant hysteresis. The PSCs with gTPA2 gave a relatively lower PCE of 7.57%, with a J_{sc} of 17.31 mA/cm^2, a V_{oc} of 0.78 V, and a FF of 0.56. The PSCs with gTPA gave the lowest PCE (5.44%), with a J_{sc} of 11.43 mA/cm^2, a V_{oc} of 0.86 V, and a FF of 0.55. We calculated the average PCE of different HTM molecular glass-based PSCs, as shown in Figure 6c−f, and the detailed parameters are summarized in Table 2. We conclude that the main reason for the low performance of gTPA-based PSCs is the low J_{sc}. Conversely, PSCs with gTPA2-OMe provided high J_{sc}, which benefits from the higher conductivity of gTPA2-OMe, which means a higher carrier transport ability. The smaller series resistance (R_s = 4.6 Ω·cm^2) also witnesses it. In addition, the

https://doi.org/10.1021/acsaem.1c02013
ACS Appl. Energy Mater. 2021, 4, 12232−12242

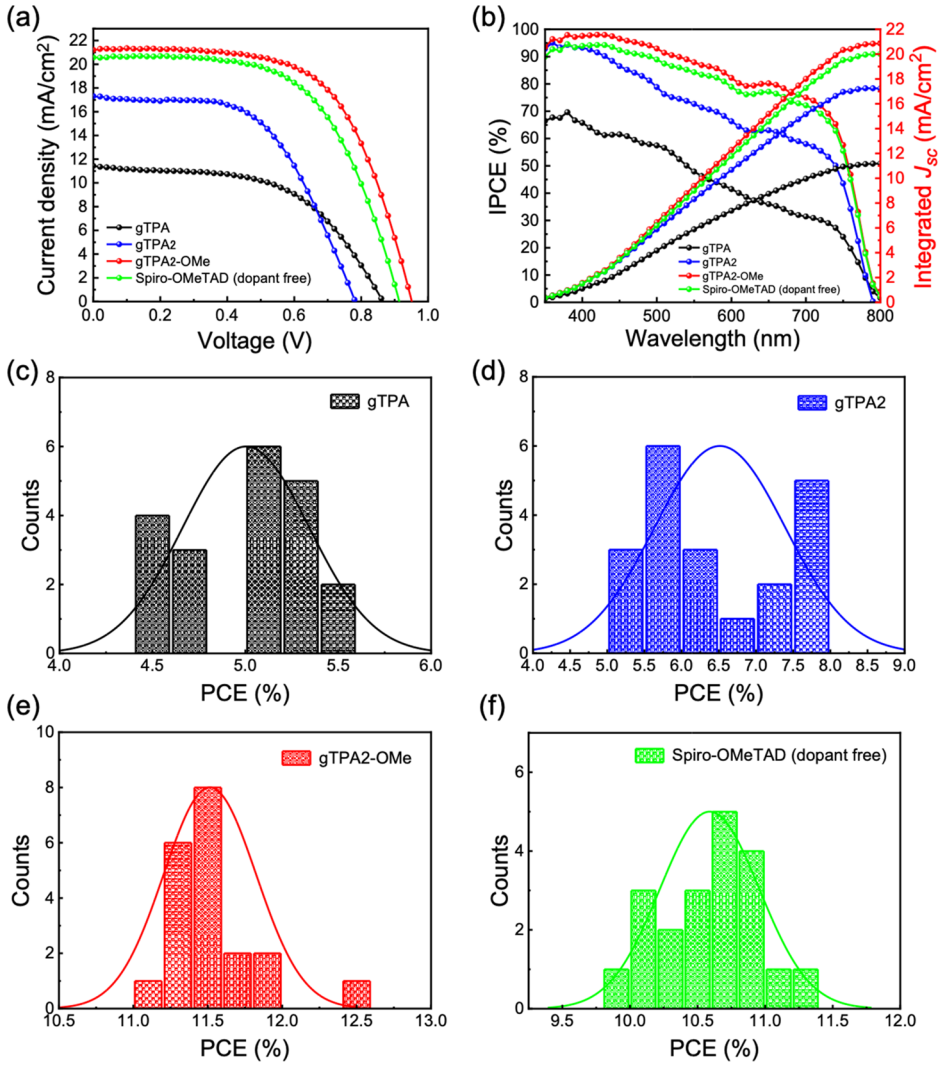

Figure 6. (a) Reverse bias $J-V$ curves, (b) IPCE spectra and integrated J_{sc} of PSCs based on dopant-free gTPA, gTPA2, gTPA2-OMe, and spiro-OMeTAD as HTMs. (c) Histograms of PCEs measured in 20 devices of gTPA. (d) Histograms of PCEs measured in 20 devices of gTPA2. (e) Histograms of PCEs measured in 20 devices of gTPA2-OMe. (f) Histograms of PCEs measured in 20 devices of spiro-OMeTAD (dopant-free).

Table 2. Photovoltaic Parameters for PSCs with Dopant-Free gTPA, gTPA2, gTPA2-OMe, and Spiro-OMeTAD HTMs

		J_{sc} (mA/cm^2)	V_{oc} (V)	FF	PCE (%)	R_s (Ω·cm^2)	R_{sh} (kΩ·cm^2)
gTPA	highest	11.43	0.86	0.55	5.44	25.2	1.1
	average	11.28 ± 0.84	0.82 ± 0.03	0.54 ± 0.02	5.00 ± 0.34		
gTPA2	highest	17.31	0.78	0.56	7.57	13.0	1.0
	average	15.41 ± 1.38	0.79 ± 0.03	0.53 ± 0.05	6.51 ± 0.88		
gTPA2-OMe	highest	21.21	0.95	0.62	12.50	4.6	1.7
	average	20.73 ± 0.27	0.92 ± 0.01	0.61 ± 0.01	11.51 ± 0.31		
spiro-OMeTAD (dopant free)	highest	20.57	0.91	0.60	11.25	7.8	1.5
	average	20.71 ± 0.73	0.91 ± 0.03	0.57 ± 0.03	10.59 ± 0.31		

larger shunt resistance (R_{sh} = 1.7 kΩ·cm^2) explains the larger V_{oc} and FF of the gTPA2-OMe device.[34,54]

From the IPCE data (Figure 6b), we see that the device based on gTPA2-OMe exhibits the highest photon−current response at 420 nm, with an EQE of 98%. To prove the accuracy of the $J-V$ measurements, we calculated the integrated current density from the IPCE spectrum, as shown in Figure 6b. The integrated current densities of the devices with gTPA, gTPA2, and gTPA2-OMe are 11.18, 17.23, and 20.86 mA/cm^2, respectively, which are in agreement with the J_{sc} values measured under standard solar AM 1.5 G illumination.[55]

We measured the current output at the maximum power point to evaluate the steady-state power output of PSCs with different HTMs. As shown in Figure 7, gTPA, gTPA2, and gTPA2-OMe-based devices maintain a very stable efficiency of 5.07, 7.19, and 12.40% for around 200 s continuous exposure to 1 sun illumination. Reproducibility of the PSCs was assessed on 20 devices, as shown in Figure S6. All devices show a relatively narrow distribution, witnessing good reproducibility.

https://doi.org/10.1021/acsaem.1c02013
ACS Appl. Energy Mater. 2021, 4, 12232−12242

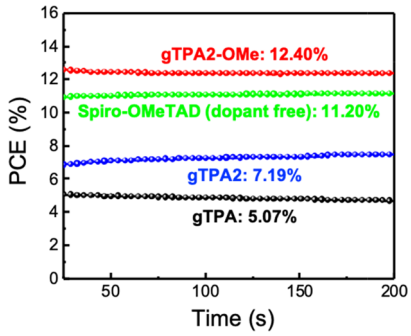

Figure 7. Steady-state efficiency at maximum power point of devices with gTPA, gTPA2, and gTPA2-OMe and spiro-OMeTAD (dopant free) under continuous AM 1.5 G illumination for around 200 s.

Device stability is an important criterion for evaluating whether PSCs can be commercially competitive. We measured the light soaking stability and long-term stability of PSCs with the different molecular glass HTMs. Unencapsulated devices were monitored under ambient conditions (AM 1.5 G illumination). The PCE of the devices with gTPA quickly decayed after 500 min. On the other hand, PSCs with gTPA2-OMe maintained around 90% of their initial performance after more than 960 min (Figure 8a). Compared with dopant-free spiro-OMeTAD, gTPA2-OMe shows a higher light soaking stability. In addition, the long-term stability in Figure 8b also shows that gTPA2-OMe-based PSCs have the best long-term stability among all others. The unencapsulated devices were stored in the dark under an air environment (40−50% relative humidity, room temperature) for over 1000 h, with no significant decrease in their original efficiency. We speculate that the increase in efficiency is due to the oxidation of molecular glass materials. The details of J_{sc}, V_{oc}, and FF parameters are summarized in Figure S7. We also summarized in Table S2 recent data from small molecule compounds used as the dopant-free HTM for the $MAPbI_3$-based PSC application. Figure 8c shows the water contact angle of each perovskite/molecular glass HTM film. Like the commonly used spiro-OMeTAD, we see that these HTMs also form a smooth and uniform film on the surface of the perovskite film (Figures 5 and S3). This shows that these HTMs are compatible with high-quality perovskite crystals, and the smooth hydrophobic surface results in the formation of a similar large water contact angle as with spiro-OMeTAD. This reveals a certain moisture-protective effect on the perovskite material, which is highly hygroscopic. Perovskite/gTPA2-OMe has the highest water contact angle of 80°, indicating that it has larger hydrophobicity, which may reduce the penetration of moisture into the perovskite layer, a cause of perovskite decomposition, thus improving the device stability (Figure 8a,b).[56,57] This may seem surprising given the fact that gTPA2-OMe possesses NH groups that can engage in hydrogen bonding. However, it has been estimated that roughly 70−80% of these NH groups is hydrogen-bonded at T_g,[58] and this fraction is even higher at ambient temperature. The result of this extensive hydrogen bonding is to further expose the hydrophobic aryl groups to the surrounding environment.

CONCLUSIONS

In summary, we synthesized three mexylaminotriazine-substituted TPA glasses via a one-step process. These three molecular glass materials showed outstanding film-forming abilities. They were incorporated as the HTM in $MAPbI_3$ PSCs. The PCE of PSCs based on gTPA2-OMe was the highest (12.50%) with an excellent device stability. The synthesized molecular-glass materials exhibit good conductivity and hole mobility. Our work proves that the molecular-glass materials synthesized with mexylaminotriazine as the core can be successfully applied as HTMs to PSCs. We do believe that the modified molecular-glass materials can completely replace spiro-OMeTAD in the future. These works are currently underway.

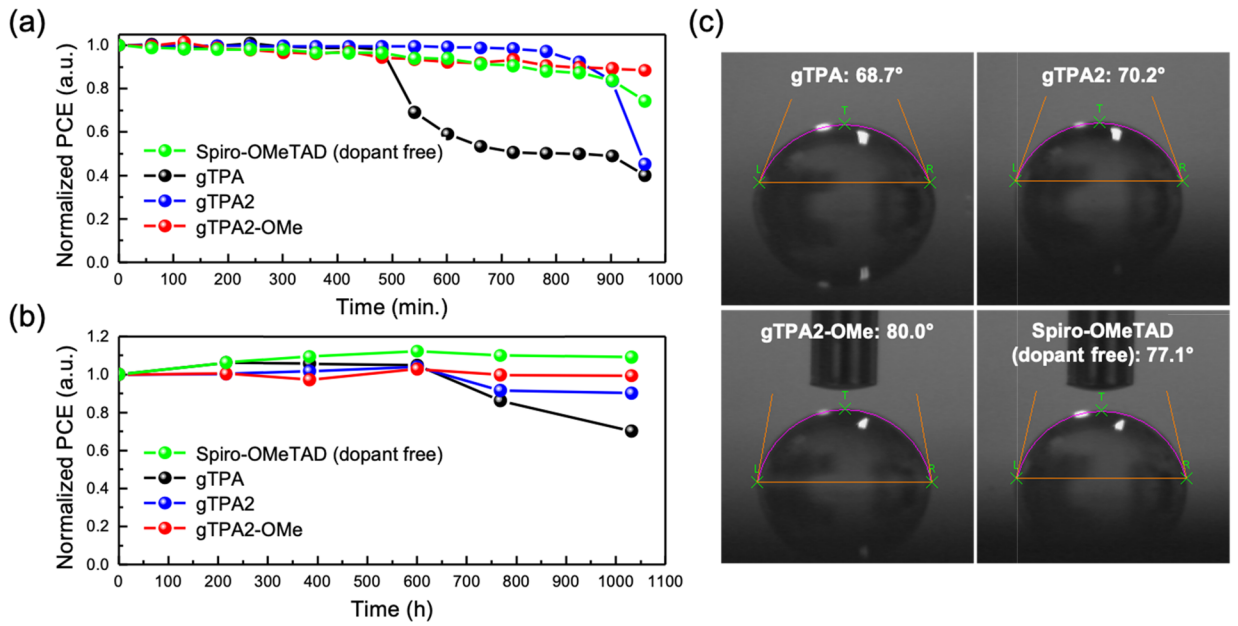

Figure 8. (a) Normalized PCE versus time (in min) on nonencapsulated devices after exposure to continuous 1 sun illumination in air with a humidity range of 40 to 50%. (b) Normalized PCE versus time (in h) of nonencapsulated devices stored in the dark under ambient air with a relative humidity range of 40 to 50%. (c) Water contact angle of the different molecular glasses.

https://doi.org/10.1021/acsaem.1c02013
ACS Appl. Energy Mater. 2021, 4, 12232−12242

■ ASSOCIATED CONTENT

Supporting Information

The Supporting Information is available free of charge at https://pubs.acs.org/doi/10.1021/acsaem.1c02013.

Image of the hole transport solutions under study; energy level diagram of the perovskite films with the HTLs under study; images of the perovskite films covered with the HTLs under study; device architecture and SEM cross-sections of the PSCs with the HTLs under study; forward and reverse current voltage characteristics of the PSCs under study; box charts of the distribution of PSC performances for the devices under study; evolution of the photovoltaic parameters of the PSCs under study with storage time under dark in air; cost analysis and summary for gTPA2-OMe; and summary of the performances of representative small molecule dopant-free HTMs for $MAPbI_3$-based PSCs (PDF)

■ AUTHOR INFORMATION

Corresponding Authors

Md. Shahiduzzaman − *Nanomaterials Research Institute, Kanazawa University, Kanazawa 920-1192, Japan;* orcid.org/0000-0002-3092-7793; Email: shahiduzzaman@se.kanazawa-u.ac.jp

Jean Michel Nunzi − *Nanomaterials Research Institute, Kanazawa University, Kanazawa 920-1192, Japan; Department of Physics, Engineering Physics and Astronomy, Department of Chemistry, Queen's University, Kingston K7L-3N6 Ontario, Canada;* orcid.org/0000-0001-5490-4273; Email: nunzijm@queensu.ca

Tetsuya Taima − *Graduate School of Frontier Science Initiative, Nanomaterials Research Institute, and Graduate School of Natural Science and Technology, Kanazawa University, Kanazawa 920-1192, Japan*; Email: taima@se.kanazawa-u.ac.jp

Authors

LiangLe Wang − *Graduate School of Frontier Science Initiative, Kanazawa University, Kanazawa 920-1192, Japan*

E. Y. Muslih − *Graduate School of Natural Science and Technology, Kanazawa University, Kanazawa 920-1192, Japan;* orcid.org/0000-0002-2972-6214

Masahiro Nakano − *Graduate School of Natural Science and Technology, Kanazawa University, Kanazawa 920-1192, Japan;* orcid.org/0000-0002-9231-4124

Makoto Karakawa − *Nanomaterials Research Institute and Graduate School of Natural Science and Technology, Kanazawa University, Kanazawa 920-1192, Japan;* orcid.org/0000-0001-7412-8179

Koji Tomita − *Department of Chemistry, School of Science, Tokai University, Hiratsuka 259-1292, Japan*

Olivier Lebel − *Department of Chemistry and Chemical Engineering, Royal Military College of Canada, Kingston K7K 7B4 Ontario, Canada;* orcid.org/0000-0002-1737-6843

Complete contact information is available at: https://pubs.acs.org/10.1021/acsaem.1c02013

Notes

The authors declare no competing financial interest.

■ ACKNOWLEDGMENTS

This study was partially financially supported by the Grant-in-Aid for Scientific Research (grant number 20H02838). This study was partially supported by the Canadian Defence Academic Research Programme (CDARP) of RMC and the Natural Sciences and Engineering Research Council of Canada Discovery Grants program (RGPIN-2020-07016).

■ REFERENCES

(1) Shahiduzzaman, M.; Fukaya, S.; Muslih, E. Y.; Wang, L.; Nakano, M.; Akhtaruzzaman, M.; Karakawa, M.; Takahashi, K.; Nunzi, J.-M.; Taima, T. Metal Oxide Compact Electron Transport Layer Modification for Efficient and Stable Perovskite Solar Cells. *Materials* **2020**, *13*, 2207.

(2) Shahiduzzaman, M.; Muslih, E. Y.; Hasan, A. K. M.; Wang, L.; Fukaya, S.; Nakano, M.; Karakawa, M.; Takahashi, K.; Akhtaruzzaman, M.; Nunzi, J.-M.; Taima, T. The Benefits of Ionic Liquids for the Fabrication of Efficient and Stable Perovskite Photovoltaics. *Chem. Eng. J.* **2021**, *411*, 128461.

(3) Burschka, J.; Pellet, N.; Moon, S.-J.; Humphry-Baker, R.; Gao, P.; Nazeeruddin, M. K.; Grätzel, M. Sequential Deposition as a Route to High-Performance Perovskite-Sensitized Solar Cells. *Nature* **2013**, *499*, 316−319.

(4) Liu, M.; Johnston, M. B.; Snaith, H. J. Efficient Planar Heterojunction Perovskite Solar Cells by Vapour Deposition. *Nature* **2013**, *501*, 395−398.

(5) Kim, H.-S.; Lee, C.-R.; Im, J.-H.; Lee, K.-B.; Moehl, T.; Marchioro, A.; Moon, S.-J.; Humphry-Baker, R.; Yum, J.-H.; Moser, J. E.; Grätzel, M.; Park, N. G. Lead Iodide Perovskite Sensitized All-Solid-State Submicron Thin Film Mesoscopic Solar Cell with Efficiency Exceeding 9%. *Sci. Rep.* **2012**, *2*, 591.

(6) Hossain, M. I.; Saleque, A. M.; Ahmed, S.; Saidjafarzoda, I.; Shahiduzzaman, M.; Qarony, W.; Knipp, D.; Biyikli, N.; Tsang, Y. H. Perovskite/Perovskite Planar Tandem Solar Cells: A Comprehensive Guideline for Reaching Energy Conversion Efficiency beyond 30%. *Nano Energy* **2021**, *79*, 105400.

(7) Shahiduzzaman, M.; Hossain, M. I.; Visal, S.; Kaneko, T.; Qarony, W.; Umezu, S.; Tomita, K.; Iwamori, S.; Knipp, D.; Tsang, Y. H. Spray Pyrolyzed TiO_2 Embedded Multi-Layer Front Contact Design for High-Efficiency Perovskite Solar Cells. *Nano-Micro Lett.* **2021**, *13*, 36.

(8) Kojima, A.; Teshima, K.; Shirai, Y.; Miyasaka, T. Organometal Halide Perovskites as Visible-Light Sensitizers for Photovoltaic Cells. *J. Am. Chem. Soc.* **2009**, *131*, 6050−6051.

(9) Im, J.-H.; Lee, C.-R.; Lee, J.-W.; Park, S.-W.; Park, N.-G. 6.5% Efficient Perovskite Quantum-Dot-Sensitized Solar Cell. *Nanoscale* **2011**, *3*, 4088−4093.

(10) Lee, M. M.; Teuscher, J.; Miyasaka, T.; Murakami, T. N.; Snaith, H. J. Efficient Hybrid Solar Cells Based on Meso-Superstructured Organometal Halide Perovskites. *Science* **2012**, *338*, 643−647.

(11) NREL. Best Research-Cell Efficiency Chart. 2021, https://www.nrel.gov/pv/cell-efficiency.html (accessed on October 8, 2021).

(12) Sanehira, E. M.; Tremolet de Villers, B. J.; Schulz, P.; Reese, M. O.; Ferrere, S.; Zhu, K.; Lin, L. Y.; Berry, J. J.; Luther, J. M. Influence of Electrode Interfaces on the Stability of Perovskite Solar Cells: Reduced Degradation Using MoO_x/Al for Hole Collection. *ACS Energy Lett.* **2016**, *1*, 38−45.

(13) Zhao, L.; Kerner, R. A.; Xiao, Z.; Lin, Y. L.; Lee, K. M.; Schwartz, J.; Rand, B. P. Redox Chemistry Dominates the Degradation and Decomposition of Metal Halide Perovskite Optoelectronic Devices. *ACS Energy Lett.* **2016**, *1*, 595−602.

(14) Zhao, D.; Sexton, M.; Park, H.-Y.; Baure, G.; Nino, J. C.; So, F. High-efficiency Solution-processed Planar Perovskite Solar Cells with a Polymer Hole Transport Layer. *Adv. Energy Mater.* **2015**, *5*, 1401855.

(15) Zhang, L.; Wu, J.; Li, D.; Li, W.; Meng, Q.; Bo, Z. Ladder-like Conjugated Polymers Used as Hole-Transporting Materials for High-

Efficiency Perovskite Solar Cells. *J. Mater. Chem. A* **2019**, *7*, 14473−14477.
(16) Xiao, J.; Shi, J.; Liu, H.; Xu, Y.; Lv, S.; Luo, Y.; Li, D.; Meng, Q.; Li, Y. Efficient $CH_3NH_3PbI_3$ Perovskite Solar Cells Based on Graphdiyne (GD)-Modified P3HT Hole-Transporting Material. *Adv. Energy Mater.* **2015**, *5*, 1401943.
(17) Shahiduzzaman, M.; Yonezawa, K.; Yamamoto, K.; Ripolles, T. S.; Karakawa, M.; Kuwabara, T.; Takahashi, K.; Hayase, S.; Taima, T. Improved Reproducibility and Intercalation Control of Efficient Planar Inorganic Perovskite Solar Cells by Simple Alternate Vacuum Deposition of PbI_2 and CsI. *ACS Omega* **2017**, *2*, 4464−4469.
(18) Cabau, L.; Garcia-Benito, I.; Molina-Ontoria, A.; Montcada, N. F.; Martin, N.; Vidal-Ferran, A.; Palomares, E. Diarylamino-Substituted Tetraarylethene (TAE) as an Efficient and Robust Hole Transport Material for 11% Methyl Ammonium Lead Iodide Perovskite Solar Cells. *Chem. Commun.* **2015**, *51*, 13980−13982.
(19) Li, H.; Fu, K.; Hagfeldt, A.; Grätzel, M.; Mhaisalkar, S. G.; Grimsdale, A. C. A Simple 3, 4-ethylenedioxythiophene Based Hole-transporting Material for Perovskite Solar Cells. *Angew. Chem.* **2014**, *126*, 4169−4172.
(20) Arora, N.; Dar, M. I.; Hinderhofer, A.; Pellet, N.; Schreiber, F.; Zakeeruddin, S. M.; Grätzel, M. Perovskite Solar Cells with CuSCN Hole Extraction Layers Yield Stabilized Efficiencies Greater than 20%. *Science* **2017**, *358*, 768−771.
(21) Rao, H.; Ye, S.; Sun, W.; Yan, W.; Li, Y.; Peng, H.; Liu, Z.; Bian, Z.; Li, Y.; Huang, C. A 19.0% Efficiency Achieved in CuO_x-Based Inverted $CH_3NH_3PbI_{3-X}Cl_x$ Solar Cells by an Effective Cl Doping Method. *Nano Energy* **2016**, *27*, 51−57.
(22) Yan, W.; Ye, S.; Li, Y.; Sun, W.; Rao, H.; Liu, Z.; Bian, Z.; Huang, C. Hole-transporting Materials in Inverted Planar Perovskite Solar Cells. *Adv. Energy Mater.* **2016**, *6*, 1600474.
(23) Kim, J. H.; Liang, P.-W.; Williams, S. T.; Cho, N.; Chueh, C.-C.; Glaz, M. S.; Ginger, D. S.; Jen, A. K.-Y. High-performance and Environmentally Stable Planar Heterojunction Perovskite Solar Cells Based on a Solution-processed Copper-doped Nickel Oxide Hole-transporting Layer. *Adv. Mater.* **2015**, *27*, 695−701.
(24) Christians, J. A.; Fung, R. C. M.; Kamat, P. V. An Inorganic Hole Conductor for Organo-Lead Halide Perovskite Solar Cells. Improved Hole Conductivity with Copper Iodide. *J. Am. Chem. Soc.* **2014**, *136*, 758−764.
(25) Qin, P.; Tanaka, S.; Ito, S.; Tetreault, N.; Manabe, K.; Nishino, H.; Nazeeruddin, M. K.; Grätzel, M. Inorganic Hole Conductor-Based Lead Halide Perovskite Solar Cells with 12.4% Conversion Efficiency. *Nat. Commun.* **2014**, *5*, 3834.
(26) Hasan, A. K. M.; Raifuku, I.; Amin, N.; Ishikawa, Y.; Sarkar, D. K.; Sobayel, K.; Karim, M. R.; Ul-Hamid, A.; Abdullah, H.; Shahiduzzaman, M.; Uraoka, Y.; Sopian, K.; Akhtaruzzaman, M. Air-Stable Perovskite Photovoltaic Cells with Low Temperature Deposited NiO_x as an Efficient Hole-Transporting Material. *Opt. Mater. Express* **2020**, *10*, 1801−1816.
(27) Hasan, A. K. M.; Sobayel, K.; Raifuku, I.; Ishikawa, Y.; Shahiduzzaman, M.; Nour, M.; Sindi, H.; Moria, H.; Rawa, M.; Sopian, K.; Amin, N.; Akhtaruzzaman, M. Optoelectronic Properties of Electron Beam-Deposited NiO_x Thin Films for Solar Cell Application. *Results Phys.* **2020**, *17*, 103122.
(28) Hossain, M. I.; Hasan, A. K. M.; Qarony, W.; Shahiduzzaman, M.; Islam, M. A.; Ishikawa, Y.; Uraoka, Y.; Amin, N.; Knipp, D.; Akhtaruzzaman, M.; Tsang, Y. H. Electrical and Optical Properties of Nickel-Oxide Films for Efficient Perovskite Solar Cells. *Small Methods* **2020**, *4*, 2000454.
(29) Urieta-Mora, J.; García-Benito, I.; Molina-Ontoria, A.; Martín, N. Hole Transporting Materials for Perovskite Solar Cells: A Chemical Approach. *Chem. Soc. Rev.* **2018**, *47*, 8541−8571.
(30) Saragi, T. P. I.; Spehr, T.; Siebert, A.; Fuhrmann-Lieker, T.; Salbeck, J. Spiro Compounds for Organic Optoelectronics. *Chem. Rev.* **2007**, *107*, 1011−1065.
(31) Matsushita, A.; Yanagida, M.; Shirai, Y.; Miyano, K. Degradation of Perovskite Solar Cells by the Doping Level Decrease of HTL Revealed by Capacitance Spectroscopy. *Sol. Energy Mater. Sol. Cells* **2021**, *220*, 110854.
(32) Choi, H.; Paek, S.; Lim, N.; Lee, Y. H.; Nazeeruddin, M. K.; Ko, J. Efficient Perovskite Solar Cells with 13.63% Efficiency Based on Planar Triphenylamine Hole Conductors. *Chem.—Eur. J.* **2014**, *20*, 10894−10899.
(33) Liu, X.; Kong, F.; Ghadari, R.; Jin, S.; Chen, W.; Yu, T.; Hayat, T.; Alsaedi, A.; Guo, F.; Tan, Z. a.; Chen, J.; Dai, S. Thiophene−Arylamine Hole-Transporting Materials in Perovskite Solar Cells: Substitution Position Effect. *Energy Technol.* **2017**, *5*, 1788−1794.
(34) Jeon, N. J.; Lee, H. G.; Kim, Y. C.; Seo, J.; Noh, J. H.; Lee, J.; Seok, S. I. O-Methoxy Substituents in Spiro-OMeTAD for Efficient Inorganic−Organic Hybrid Perovskite Solar Cells. *J. Am. Chem. Soc.* **2014**, *136*, 7837−7840.
(35) Rakstys, K.; Abate, A.; Dar, M. I.; Gao, P.; Jankauskas, V.; Jacopin, G.; Kamarauskas, E.; Kazim, S.; Ahmad, S.; Grätzel, M.; Nazeeruddin, M. K. Triazatruxene-Based Hole Transporting Materials for Highly Efficient Perovskite Solar Cells. *J. Am. Chem. Soc.* **2015**, *137*, 16172−16178.
(36) Magomedov, A.; Paek, S.; Gratia, P.; Kasparavicius, E.; Daskeviciene, M.; Kamarauskas, E.; Gruodis, A.; Jankauskas, V.; Kantminiene, K.; Cho, K. T.; Rakstys, K.; Malinauskas, T.; Getautis, V.; Nazeeruddin, M. K. Diphenylamine-substituted Carbazole-based Hole Transporting Materials for Perovskite Solar Cells: Influence of Isomeric Derivatives. *Adv. Funct. Mater.* **2018**, *28*, 1704351.
(37) Eren, R. N.; Plante, A.; Meunier, A.; Laventure, A.; Huang, Y.; Briard, J. G.; Creber, K. J.; Pellerin, C.; Soldera, A.; Lebel, O. One Ring to Rule Them All: Effect of Aryl Substitution on Glass-Forming Ability in Mexylaminotriazine Molecular Glasses. *Tetrahedron* **2012**, *68*, 10130−10144.
(38) Adhikari, T.; Shahiduzzaman, M.; Yamamoto, K.; Lebel, O.; Nunzi, J.-M. Interfacial Modification of the Electron Collecting Layer of Low-Temperature Solution-Processed Organometallic Halide Photovoltaic Cells Using an Amorphous Perylenediimide. *Sol. Energy Mater. Sol. Cells* **2017**, *160*, 294−300.
(39) Adhikari, T.; Bobbara, S. R.; Nunzi, J.-M.; Lebel, O. Efficiency Enhancement of Ternary Blend Organic Photovoltaic Cells with Molecular Glasses as Guest Acceptors. *Org. Electron.* **2018**, *53*, 74−82.
(40) Wang, L.; Shahiduzzaman, M.; Fukaya, S.; Muslih, E. Y.; Nakano, M.; Karakawa, M.; Takahashi, K.; Tomita, K.; Lebel, O.; Nunzi, J. M.; Taima, T. Low-Cost Molecular Glass Hole Transport Material for Perovskite Solar Cells. *Jpn. J. Appl. Phys.* **2021**, *60*, SBBF12.
(41) Zheng, M.; Bai, F.; Zhu, D. New Light Emitting Materials: Alternating Copolymers with Hole Transport and Emitting Chromophores. *J. Appl. Polym. Sci.* **1999**, *74*, 3351−3358.
(42) Chang, C.-W.; Chung, C.-H.; Liou, G.-S. Novel Anodic Polyelectrochromic Aromatic Polyamides Containing Pendent Dimethyltriphenylamine Moieties. *Macromolecules* **2008**, *41*, 8441−8451.
(43) Shahiduzzaman, M.; Wang, L.; Fukaya, S.; Muslih, E. Y.; Kogo, A.; Nakano, M.; Karakawa, M.; Takahashi, K.; Tomita, K.; Nunzi, J.-M.; Miyasaka, T.; Taima, T. Ionic Liquid-Assisted $MAPbI_3$ Nanoparticle-Seeded Growth for Efficient and Stable Perovskite Solar Cells. *ACS Appl. Mater. Interfaces* **2021**, *13*, 21194−21206.
(44) Niu, G.; Yu, H.; Li, J.; Wang, D.; Wang, L. Controlled Orientation of Perovskite Films through Mixed Cations toward High Performance Perovskite Solar Cells. *Nano Energy* **2016**, *27*, 87−94.
(45) Shahiduzzaman, M.; Kulkarni, A.; Visal, S.; Wang, L.; Nakano, M.; Karakawa, M.; Takahashi, K.; Umezu, S.; Masuda, A.; Iwamori, S.; Isomura, M.; Miyasaka, T.; Tomita, K.; Taima, T. A Single-Phase Brookite TiO_2 Nanoparticle Bridge Enhances the Stability of Perovskite Solar Cells. *Sustainable Energy Fuels* **2020**, *4*, 2009−2017.
(46) Wang, L.; Shahiduzzaman, M.; Muslih, E. Y.; Nakano, M.; Karakawa, M.; Takahashi, K.; Tomita, K.; Nunzi, J. M.; Taima, T. Double-Layer CsI Intercalation into an $MAPbI_3$ Framework for Efficient and Stable Perovskite Solar Cells. *Nano Energy* **2021**, *86*, 106135.

https://doi.org/10.1021/acsaem.1c02013
ACS Appl. Energy Mater. 2021, 4, 12232−12242

(47) de Bettignies, R.; Nicolas, Y.; Blanchard, P.; Levillain, E.; Nunzi, J.-M.; Roncali, J. Planarized Star-shaped Oligothiophenes as a New Class of Organic Semiconductors for Heterojunction Solar Cells. *Adv. Mater.* **2003**, *15*, 1939−1943.
(48) Amal, M. I.; Kim, K. H. Structural and Optical Properties of Sulfurized Cu_2ZnSnS_4 Thin Films from Cu−Zn−Sn Alloy Precursors. *J. Mater. Sci.: Mater. Electron.* **2013**, *24*, 559−566.
(49) Amal, M. I.; Kim, K. H. Optical Properties of Selenized $Cu_2ZnSnSe_4$ Films from a Cu-Zn-Sn Metallic Precursor. *Chalcogenide Lett.* **2012**, *9*, 345−353.
(50) Huang, P.; Manju; Kazim, S.; Sivakumar, G.; Salado, M.; Misra, R.; Ahmad, S. Pyridine Bridging Diphenylamine-Carbazole with Linking Topology as Rational Hole Transporter for Perovskite Solar Cells Fabrication. *ACS Appl. Mater. Interfaces* **2020**, *12*, 22881−22890.
(51) Poplavskyy, D.; Nelson, J. Nondispersive Hole Transport in Amorphous Films of Methoxy-Spirofluorene-Arylamine Organic Compound. *J. Appl. Phys.* **2003**, *93*, 341−346.
(52) Singh, A.; Abate, S. Y.; Pavan Kumar, C.; Wu, W.-T.; Hsiao, J.-C.; Wu, F.-L.; Lin, J. T. s.; Tao, Y.-T. Bis (Diphenylamine)-Tethered Carbazolyl Anthracene Derivatives as Hole-Transporting Materials for Stable and High-Performance Perovskite Solar Cells. *ACS Appl. Energy Mater.* **2020**, *3*, 10752−10764.
(53) Habisreutinger, S. N.; Noel, N. K.; Snaith, H. J. Hysteresis Index: A Figure without Merit for Quantifying Hysteresis in Perovskite Solar Cells. *ACS Energy Lett.* **2018**, *3*, 2472−2476.
(54) Shen, C.; Wu, Y.; Zhang, H.; Li, E.; Zhang, W.; Xu, X.; Wu, W.; Tian, H.; Zhu, W. H. Semi-Locked Tetrathienylethene as a Building Block for Hole-Transporting Materials: Toward Efficient and Stable Perovskite Solar Cells. *Angew. Chem., Int. Ed.* **2019**, *58*, 3784−3789.
(55) Sidhik, S.; Pasarán, A. C.; Pérez, C. R.; López-Luke, T.; De la Rosa, E. Modulating the Grain Size, Phase and Optoelectronic Quality of Perovskite Films with Cesium Iodide for High-Performance Solar Cells. *J. Mater. Chem. C* **2018**, *6*, 7880−7889.
(56) Zheng, L.; Chung, Y.-H.; Ma, Y.; Zhang, L.; Xiao, L.; Chen, Z.; Wang, S.; Qu, B.; Gong, Q. A Hydrophobic Hole Transporting Oligothiophene for Planar Perovskite Solar Cells with Improved Stability. *Chem. Commun.* **2014**, *50*, 11196−11199.
(57) Liu, X.; Kong, F.; Cheng, T.; Chen, W.; Tan, Z. a.; Yu, T.; Guo, F.; Chen, J.; Yao, J.; Dai, S. Tetraphenylmethane-Arylamine Hole-Transporting Materials for Perovskite Solar Cells. *ChemSusChem* **2017**, *10*, 968−975.
(58) Laventure, A.; De Grandpré, G.; Soldera, A.; Lebel, O.; Pellerin, C. Unraveling the Interplay between Hydrogen Bonding and Rotational Energy Barrier to Fine-Tune the Properties of Triazine Molecular Glasses. *Phys. Chem. Chem. Phys.* **2016**, *18*, 1681−1692.

https://doi.org/10.1021/acsaem.1c02013
ACS Appl. Energy Mater. 2021, 4, 12232−12242